Published in final edited form as:
Neuroimage. 2013 May 15; 72: 41–47. doi:10.1016/j.neuroimage.2013.01.038.

A robust multi-shot scan strategy for high-resolution diffusion weighted MRI enabled by multiplexed sensitivity-encoding (MUSE)

Nan-kuei Chen[*], **Arnaud Guidon**, **Hing-Chiu Chang**, and **Allen W. Song**
Brain Imaging and Analysis Center, Duke University Medical Center

Abstract

Diffusion weighted magnetic resonance imaging (DWI) data have been mostly acquired with single-shot echo-planar imaging (EPI) to minimize motion induced artifacts. The spatial resolution, however, is inherently limited in single-shot EPI, even when the parallel imaging (usually at an acceleration factor of 2) is incorporated. Multi-shot acquisition strategies could potentially achieve higher spatial resolution and fidelity, but they are generally susceptible to motion-induced phase errors among excitations that are exacerbated by diffusion sensitizing gradients, rendering the reconstructed images unusable. It has been shown that shot-to-shot phase variations may be corrected using navigator echoes, but at the cost of imaging throughput. To address these challenges, a novel and robust multi-shot DWI technique, termed multiplexed sensitivity-encoding (MUSE), is developed here to reliably and inherently correct nonlinear shot-to-shot phase variations without the use of navigator echoes. The performance of the MUSE technique is confirmed experimentally in healthy adult volunteers on 3 Tesla MRI systems. This newly developed technique should prove highly valuable for mapping brain structures and connectivities at high spatial resolution for neuroscience studies.

Keywords

diffusion weighted imaging; inherent phase correction; multiplexed sensitivity-encoding; interleaved echo-planar imaging; multi-shot echo-planar imaging

Introduction

Diffusion-weighted magnetic resonance imaging (DWI) techniques, including diffusion tensor imaging (DTI), are now among the most powerful tools for assessing the neuronal microstructures in vivo (Le Bihan et al. (1988); Moseley et al. (1990); Basser et al. (1994)). To date, DWI data have been commonly acquired with single-shot pulse sequences, such as single-shot echo-planar imaging (EPI) (Turner et al. (1991)), to avoid significant artifacts resulting from amplified motion-induced phase errors (Anderson and Gore (1994)). However, single-shot DWI is often limited in spatial resolution (Farzaneh et al. (1990)),

[*]Correspondence should be addressed to: Nan-kuei Chen, Ph.D. Brain Imaging and Analysis Center, Duke University Medical Center, Box 2737, Hock Plaza Durham, NC 27710, Phone: (919) 613-6207, Fax: (919) 681-7033, nankuei.chen@duke.edu.

making it difficult to measure detailed diffusion properties in fine structures where high spatial resolution is required (Jezzard et al. (1998)).

Significant efforts have been invested to address the resolution limitation in DWI. Advances in parallel imaging techniques have enabled higher spatial resolution and fidelity using under-sampled k-space data at a chosen acceleration factor (Griswold et al. (2002)). However, when using a lower acceleration factor (e.g., 2), parallel DWI is still limited by geometric distortions and the less-than-ideal point-spread-function. On the other hand, when using a higher acceleration factor, the noise is undesirably amplified in reconstructed parallel MR images. To uproot these limitations, multi-shot techniques such as interleaved EPI, interleaved spiral imaging, PROPELLER, and fast spin-echo pulse sequences with embedded or inherent low-resolution navigator echoes have been developed to address the amplified shot-to-shot motion-induced phase variations, and produce adequate high resolution DWI data (Butts et al. (1996); Bammer et al. (1999); Atkinson et al. (2000); Pipe et al. (2002); Wang et al. (2005); Skare et al. (2006); Atkinson et al. (2006); Porter and Heidemann (2009); Li et al. (2011); Jeong et al. (2012)). However, navigator-echo based correction can fail if the motions differ between the navigation and the actual DWI data acquisition. Alternative phase correction schemes without using navigator echoes have also been proposed. For example, it has been shown that the linear terms of motion-induced phase errors may be estimated from interleaved DWI with an iterative, and often time-consuming, computation algorithm in post-processing without navigation (Robson et al. (1997)). However, this iterative computation framework may not be effective in correcting nonlinear phase errors resulting from local motions in multi-shot DWI data. It has been shown that linear and nonlinear phase variations in multi-shot DWI can be inherently estimated from the embedded low-resolution signals of variable-density spiral imaging (Miller and Pauly (2003); Liu et al. (2004); Frank et al. (2010)). A potential concern with the variable-density spiral imaging methods is that the imaging throughput may be compromized when a high-resolution navigator echo is desired.

To address the aforementioned technical challenges, we report here a novel interleaved DWI technique, enabled by multiplexed sensitivity-encoding (MUSE), to achieve high spatial resolution, high SNR, high spatial fidelity, and minimal motion-induced phase errors - all inherently without the need for navigator echoes. The developed MUSE method first uses the conventional SENSE technique (Pruessmann et al. (1999)) to estimate the motion-induced phase variations among multiple EPI segments, and then jointly calculates the magnitude signals of aliased voxels (due to intra-scan motion) simultaneously from all segments of interleaved EPI. In comparison to the conventional SENSE procedure, the MUSE method has a greatly improved matrix inversion conditioning and thus can produce DWI images at higher SNR. As compared with existing navigator-based interleaved DWI methods, our technique enables interleaved DWI without any pulse sequence modification.

Theory

DWI data obtained with an interleaved EPI pulse sequence are highly susceptible to aliasing artifacts as the result of amplified shot-to-shot motion-induced phase variations in the presence of strong diffusion weighting gradients. Here, without loss of generality for multi-shot acquisitions, we discuss a simplified procedure for reconstructing aliasing-free images from DWI data obtained with a 2-shot interleaved EPI sequence using a three-channel coil. This procedure can be readily adapted to more interleaves and larger coil arrays, as shown in our experimental results. Aliased images obtained from the first and second segments of 2-shot interleaved EPI are represented by Equations 1 and 2, respectively, where u_j are aliased signals detected by the j-th coil ($j = 1, 2, 3$) from the first EPI segment; v_j are aliased signals detected by the j-th coil ($j = 1, 2, 3$) from the second EPI segment; S_j are the coil sensitivity

profiles for the j-th coil; and p and q are un-aliased full-FOV images that we plan to reconstruct.

$$u_j(x,y)=S_j(x,y)p(x,y)+S_j(x,y+\frac{FOV_y}{2})p(x,y+\frac{FOV_y}{2}) \quad (1)$$

$$v_j(x,y)=S_j(x,y)q(x,y)-S_j(x,y+\frac{FOV_y}{2})q(x,y+\frac{FOV_y}{2}) \quad (2)$$

Note that the sign before the $S_j(x,y+\frac{FOV_y}{2})$ term differs between Equations 1 and 2, because of the relative k-space trajectory shift between two EPI segments. With known coil sensitivity profiles, one can estimate unaliased full-FOV images from the acquired aliased signals using parallel MRI reconstruction. For example, the full-FOV image p can be calculated from the first EPI segment using the SENSE technique (Pruessmann et al. (1999)), where the two unknowns (i.e., $p(x, y)$ and $p(x,y+\frac{FOV_y}{2})$) are determined from the three measured signals (i.e., $u_j(x, y)$ with $j = 1, 2, 3$). Similarly, the full-FOV image q can be calculated from the second EPI segment with SENSE. Note that the full-FOV images p and q differ mainly by the motion-induced phase inconsistencies between the two shots, as shown in Equations 3 and 4, where the nonnegative real number D represents the magnitude signal (i.e., the proton-density weighted by diffusion contrast) that is expected to be consistent across multiple EPI segments; θ and φ are the motion-induced phase errors that differ between the two shots; and c represents the background phase value that is independent of motion. The full-FOV images estimated by the SENSE method (p_s and q_s) can be represented by Equations 5 and 6, where n_p and n_q are the SENSE-produced noises that are usually significant when the number of unknowns (i.e., 2 in this example) is not much smaller than the number of equations (i.e., 3 in this example).

$$p(x,y)=D(x,y)e^{i\theta(x,y)+c(x,y)} \quad (3)$$

$$q(x,y)=D(x,y)e^{i\varphi(x,y)+c(x,y)} \quad (4)$$

$$p_s(x,y)=p(x,y)+n_p(x,y) \quad (5)$$

$$q_s(x,y)=q(x,y)+n_q(x,y) \quad (6)$$

Even though the full-FOV images estimated by the SENSE method are susceptible to undesirable noise amplification, the shot-to-shot phase inconsistencies, which are expected to be spatially smooth, can be reliably estimated with Equations 7 and 8, where TV represents the denoising operation based on total variation (Rudin et al. (1992)).

$$e^{i\theta(x,y)+c(x,y)} \cong \frac{TV(p_s(x,y))}{|TV(p_s(x,y))|} \quad (7)$$

$$e^{i\varphi(x,y)+c(x,y)} \cong \frac{TV(q_s(x,y))}{|TV(q_s(x,y))|} \quad (8)$$

At this point, Equations 1 and 2 can be reformatted to Equations 9 and 10.

$$u_j(x,y)=\left[S_j(x,y)\frac{TV(p_s(x,y))}{|TV(p_s(x,y))|}\right]D(x,y)+\left[S_j(x,y+\frac{FOV_y}{2})\frac{TV(p_s(x,y+\frac{FOV_y}{2}))}{\left|TV(p_s(x,y+\frac{FOV_y}{2}))\right|}\right]D(x,y+\frac{FOV_y}{2}) \quad (9)$$

$$v_j(x,y)=\left[S_j(x,y)\frac{TV(q_s(x,y))}{|TV(q_s(x,y))|}\right]D(x,y)-\left[S_j(x,y+\frac{FOV_y}{2})\frac{TV(q_s(x,y+\frac{FOV_y}{2}))}{\left|TV(q_s(x,y+\frac{FOV_y}{2}))\right|}\right]D(x,y+\frac{FOV_y}{2}) \quad (10)$$

It can be seen that Equations 9 and 10 have two common unknowns (i.e., $D(x, y)$ and $D(x,y+\frac{FOV_y}{2})$), and thus can be solved jointly when the information on motion-induced phase errors (e.g., $\frac{TV(p_s(x,y))}{|TV(p_s(x,y))|}$) is incorporated. The above described procedure, termed multiplexed sensitivity encoding (MUSE), has a significantly improved matrix inversion condition (with 2 unknowns and 6 equations in this example) as compared with the conventional SENSE procedure (with 2 unknowns and 3 equations in this example). Even though the concept of MUSE procedure is explained here with 2-shot EPI as an example, the MUSE framework can be directly extended to interleaved EPI with a larger number of segments. It should be noted that the multiplexed sensitivity encoding method is a pure post-processing procedure, without requiring hardware or pulse sequence modification, and is different from the recently developed multiplexed EPI pulse sequence (Feinberg et al. (2010)).

Methods

A series of experiments were conducted on 3 Tesla MRI systems (GEHC HD and MR750, Waukesha, WI) to evaluate the developed MUSE method, as described below.

A) To evaluate the performance of the developed technique, DTI images ($0.86 \times 0.86 \times 4mm^3$) were obtained from 6 healthy volunteers using an 8-channel receiver coil. DTI images (with one baseline acquisition, and 15 diffusion weighting directions at a b factor of either $500\frac{sec}{mm^2}$ or $1000\frac{sec}{mm^2}$) were acquired using a 4-shot interleaved EPI pulse sequence with a twice-refocused spin-echo scheme to minimize the eddy current induced geometric distortions (Reese et al. (2003)). Scan parameters included: number of partial-Fourier over-sampling *ky* lines 12, in-plane acquisition matrix size 256 × 140 (i.e., 256 × 256 after partial-Fourier reconstruction for a 4-shot scan), FOV $22 \times 22cm^2$, axial-plane slice thickness 4mm, TR 5 sec, and TE 59.3 msec.

The acquired data were processed with the following steps. First, the recently developed phase-cycled reconstruction procedure (Chen et al. (2011)) was used to measure the 2D phase errors resulting from odd-even echo inconsistencies in the baseline (i.e. T2-weighted) image, and the measured information was then used to suppress the Nyquist artifacts in both baseline and diffusion-weighted images. Second, the coil-sensitivity profiles were estimated from the baseline T2-weighted images. Third, using the conventional SENSE reconstruction procedure, four full-FOV images were reconstructed from four DWI segments, and the shot-

to-shot phase variations were calculated with Equation 7, where the total variation algorithm was used to smooth the complex images and phase-unwrapping was not needed. Fifth, the smoothed phase maps (step 4) and the coil sensitivity profiles (step 2) were used to reconstruct aliasing-free DWI images from the Nyquist-corrected DWI data, using the MUSE algorithm. Sixth, the eigenvectors and the fractional anisotropy (FA) values were calculated from the aliasing-free DTI data. Seventh, in order to illustrate the noise reduction and SNR improvement as an advantage by the MUSE procedure, another set of aliasing-free DTI data was generated by summing the phase-corrected maps derived from four EPI segments with the conventional SENSE procedure (i.e., in step 3 described above) (Holdsworth et al. (2012)), and the quality of the resultant FA maps were then assessed in terms of the tensor fitting residual errors (Andersson and Skare (2002); Mohammadi et al. (2010)).

B) To test the capability of achieving high in-plane spatial-resolution with the MUSE technique, DWI ($0.375 \times 0.375 \times 5 mm^3$) and DTI ($0.3 \times 0.3 \times 8 mm^3$) data were acquired with 4-shot interleaved EPI from a healthy volunteer. The DWI data set, consisting of 1 baseline image and 3 images with diffusion gradients at $b=800 \frac{sec}{mm^2}$ applied along three orthogonal directions, was obtained using an 8-channel coil with the following parameters: number of partial-Fourier over-sampling *ky* lines 12, in-plane acquisition matrix size 512 × 268 (i.e., 512 × 512 after partial-Fourier reconstruction for a 4-shot scan), FOV 19.2 × $19.2 cm^2$, axial-plane slice thickness 5mm, TR 6.5 sec, and TE 74.3 msec. The DTI data set, consisting of 4 baseline images and 15 DWI at $b=500 \frac{sec}{mm^2}$, was obtained using an 8-channel coil with these scan parameters: number of partial-Fourier over-sampling *ky* lines 12, in-plane acquisition matrix size 512 × 268 (i.e., 512 × 512 after partial-Fourier reconstruction for a 4-shot scan), FOV $15.3 \times 15.3 cm^2$, axial-plane slice thickness 8mm, TR 5 sec, and TE 75.5 msec. The developed MUSE method was used to reconstruct high-resolution DWI and DTI maps, as described in A).

C) To test the reliability of the MUSE method for processing data at different SNR levels, 7 DWI data sets were acquired from a healthy volunteer using an 8-channel coil with b factors of 500, 750, 1000, 1250, 1500, 1750 and $2000 \frac{sec}{mm^2}$. Each DWI data set consisted of 1 baseline image and 3 images with diffusion gradients applied along three orthogonal directions. Scan parameters included: number of partial-Fourier over-sampling *ky* lines 12, in-plane acquisition matrix size 384 × 204 (i.e., 384 × 384 after partial-Fourier reconstruction for a 4-shot scan), FOV 19.2 × $19.2 cm^2$, axial-plane slice thickness 4mm, TR 5 sec, and TE ranging from 61.7 to 87 msec. Images reconstructed with the MUSE method and the conventional SENSE procedure were compared in terms of the white-matter coefficient of variation (i.e., the ratio of standard deviation to the mean signal intensity within white-matter ROIs).

D) To further assess the inherent SNR penalty resulting from either MUSE or SENSE reconstruction, three sets of 4-shot spin-echo EPI data (without diffusion sensitizing gradients) were acquired from a healthy volunteer using different receiver coils: 8-channel GE coil; 32-channel GE coil; and 32-channel NOVA coil. Additionally, a 2-shot EPI data set was acquired with an 8-channel GE coil. Scan parameters included: number of partial-Fourier over-sampling *ky* lines 12, in-plane acquisition matrix size 256 × 140 (i.e., 256 × 256 after partial-Fourier reconstruction for a 4-shot scan), FOV 22 × $22 cm^2$, axial-plane slice thickness 4mm, TR 5 sec, and TE 59.3 msec. Without applying diffusion-sensitizing gradients, interleaved EPI images reconstructed directly with 2D FFT (after Nyquist artifact removal) were free from motion-induced aliasing artifact, and thus could be used as the reference to quantify the SNR penalty in either MUSE or SENSE reconstruction.

Results

Using the new MUSE procedure, the aliasing artifacts in interleaved EPI based DWI can always be reliably removed, as confirmed from all the acquired data, and the produced images have higher SNR as compared with the SENSE-produced images, as summarized below.

A) Figure 1a shows the Nyquist-corrected DWI images produced by the conventional interleaved EPI reconstruction (i.e., a direct k-space data combination followed by 2D FFT), corresponding to 15 directions obtained from one representative participant. As expected, the levels of motion-induced aliasing artifacts vary significantly, depending on the degree of intrascan motion. The ghost-to-signal ratio (GSR) is 0.36 ± 0.13 in images shown in Figure 1a. Figure 1b shows that the motion-induced aliasing artifacts can be effectively eliminated using MUSE, regardless of the levels of aliasing artifacts in the raw DWI data. The GSR is 0.08 ± 0.01 in images shown in Figure 1b. It should be noted that even though the motion-induced aliasing artifacts can also be reduced (GSR: 0.19 ± 0.01) with a conventional SENSE procedure, the resultant images have significantly lower SNRs. Figures 1c and 1d compare the FA maps produced with the conventional SENSE reconstruction (i.e., the combination of 4 images produced by applying SENSE to individual segments: Holdsworth et al. (2012)) and the new MUSE technique, respectively. Further analyses showed that, for white-matter voxels in this slice, the tensor fitting residual errors achieved with the MUSE method was 53% of that from the conventional SENSE reconstruction (Andersson and Skare (2002); Mohammadi et al. (2010)). It is demonstrated that MUSE-enabled DWI has a significantly lower noise level as the result of improved conditioning for matrix inversion.

Figures 2a and 2b show the DTI images before and after applying the MUSE procedure, respectively, for another slice that includes the brainstem and eyes where local motion artifacts are prevalent. It can be seen that, because of the local motion, the aliasing artifacts can be highly significant in many of the interleaved DWI images (Figure 2a, GSR: 0.36±0.22). Furthermore, the aliased signals of the eyes may destructively interfere with the brain images. These aliasing artifacts can all be effectively eliminated by the MUSE procedure, as demonstrated in Figure 2b (GSR: 0.05 ± 0.01). Again, even though the motion-induced aliasing artifact can also be suppressed (GSR: 0.13±0.01) with the conventional SENSE reconstruction, the resultant DTI images and FA map have lower SNR (Figure 2c) as compared with the MUSE produced results (Figure 2d). For white-matter voxels in this slice, the tensor fitting residual errors (Andersson and Skare (2002); Mohammadi et al. (2010)) achieved with the MUSE method was 69% of that from the conventional SENSE reconstruction.

For a 2D 4-shot EPI of 256 × 256 matrix obtained with an 8-channel coil, the data processing time was about 83 sec (including 20 sec for an iterative 2D phase-cycled reconstruction and Nyquist artifact removal; 17 sec for initial SENSE estimation of shot-to-shot phase variation, 10 sec for the total variation based noise reduction, and 36 sec for the final MUSE reconstruction) with Matlab programs running in an Apple Macbook Pro (2.7 GHz intel core i7 CPU; 8GB DDR3 memory). Note that the computation time can be reduced by performing pre-processing steps (including 2D phase-cycled reconstruction, initial SENSE based estimation of shot-to-shot phase variation, and total variation based smoothing) only in the central portion of the k-space data. For example, if the pre-processing steps were carried in the central 64 × 64 k-space matrix and the calculated phase errors maps were subsequently interpolated to 256 × 256 matrices for the final MUSE reconstruction, then the total data processing time was about 50 sec per slice (including 4 sec for an iterative 2D phase-cycled reconstruction and Nyquist artifact removal; 3 sec for

initial SENSE estimation of shot-to-shot phase variation, 7 sec for the total variation based noise reduction, and 36 sec for the MUSE reconstruction).

B) Figure 3a shows a MUSE-based DWI image at high in-plane resolution (voxel size: $0.375 \times 0.375 \times 5 mm^3$; matrix size: 512 × 512), where fine anatomic features are visible. In contrast, the low-resolution version of the same image (Figure 3b: voxel size: $1.5 \times 1.5 \times 5 mm^3$; matrix size: 128 × 128), reconstructed from only the central portion of the k-space data, has significantly lower anatomic resolvability (as indicated by arrows). Figure 4a shows an FA map with high in-plane resolution ($0.3 \times 0.3 \times 8 mm^3$) generated by the developed MUSE method. The voxels inside the white box are displayed in Figure 4b, where distinct FA patterns, likely between white matter and gray matter (indicated by green and red arrows), are visible. Figures 4c and d show the contours of the indicated green and red voxels overlaid onto the mean DWI and T2*-weighted EPI maps (i.e., the non-diffusion-weighted baseline EPI), respectively, suggesting that white and gray matter FA patterns can be differentiated with the MUSE-based high-resolution DTI. Images shown in Figures 3 and 4 indicate that the developed MUSE method enables high-resolution DWI and can provide information that is usually not available at low in-plane spatial-resolution.

C) Figures 5a and b compare the MUSE- and SENSE-produced DWI maps corresponding to b factors ranging from 500 to $2000 \frac{sec}{mm^2}$ at a $250 \frac{sec}{mm^2}$ step. It can be seen that the motion-induced aliasing artifacts can all be effectively removed with the MUSE method regardless of the SNR level, and the MUSE method is less susceptible to undesirable noise amplification as compared with the SENSE reconstruction. The magnitude average of all 7 MUSE-DWI and the magnitude average of all SENSE-DWI are shown in Figures 5c and d, respectively, for an easy visualization of the SNR difference between these two reconstruction methods. The white-matter coefficient of variation (i.e., the ratio of standard deviation to the mean signals in a white-matter ROIs) in images reconstructed with the MUSE and SENSE methods are shown by black and yellow bars, respectively, in Figure 5e. The SNR values for the MUSE-based DWI images, measured by the ratio of white-matter signals to the background noises, are 8.5, 6.5, 5.0, 3.9, 3.4, 2.9, and 2.4. These data suggest that the MUSE reconstruction is superior to conventional SENSE reconstruction even for DWI data with very low SNR.

D) Non-diffusion-weighted interleaved EPI images reconstructed directly with 2D FFT were used as the reference to measure the SNR penalty resulting from either MUSE or SENSE reconstruction. First, for data obtained with an 8-channel GE coil, the white-matter coefficient of variation in 4-shot MUSE images was 3.1% higher than that obtained with 2D FFT, and the white-matter coefficient of variation in 4-shot SENSE images was 23.3% higher than that obtained with 2D FFT. Second, with the same 8-channel GE coil, the white-matter coefficient of variation in 2-shot MUSE images was 0.4% higher than that obtained with 2D FFT, and the white-matter coefficient of variation in 2-shot SENSE images was 14.6% higher than that obtained with 2D FFT. Third, for data obtained with a 32-channel GE coil, the white-matter coefficient of variation in 4-shot MUSE images was 1.2% higher than that obtained with 2D FFT, and the white-matter coefficient of variation in 4-shot SENSE images was 16.7% higher than that obtained with 2D FFT. Fourth, using a 32-channel NOVA coil, the white-matter coefficient of variation in 4-shot MUSE images was 8.5% higher than that obtained with 2D FFT, and the white-matter coefficient of variation in 4-shot SENSE images was 41.0% higher than that obtained with 2D FFT. These data suggest that the SNR penalty resulting from the MUSE reconstruction is generally not significant for 2-shot and 4-shot EPI, and is always smaller as compared with the SENSE reconstruction.

Discussion and Conclusions

A general and effective approach to enable high-resolution DWI through multi-shot acquisitions, termed MUSE, is presented in this report. The developed MUSE technique produces multi-shot DWI data with higher spatial resolution and fidelity, as compared with single-shot acquisition. In comparison to the conventional navigator-based interleaved DWI, the new MUSE technique, which requires neither navigator nor reference echoes, also has several advantages. First, the imaging throughput of navigator-less interleaved DWI is higher than that of navigator-based interleaved DWI. Second, unlike navigator-based correction which could fail when the motions differ between navigation, the newly developed MUSE method can inherently measure and correct phase errors. Similar to the variable-density spiral imaging based DWI (Miller and Pauly (2003); Liu et al. (2004); Frank et al. (2010)), our MUSE method is capable of inherently estimating both linear and nonlinear phase variations directly from the acquired multi-shot DWI data, but without requiring any pulse sequence modification.

A limitation of the MUSE method is that the number of EPI segments cannot be higher than the number of coils, otherwise the phase variation maps cannot be estimated with the conventional SENSE procedure (i.e., step 3 described in the Methods section). It should be noted that, as compared with the conventional SENSE reconstruction, the MUSE procedure has an improved matrix inversion conditioning even when the number of EPI segments is not significantly smaller than the number of coils. For example, as demonstrated in our human brain data, robust high-resolution DWI can be obtained from a 4-shot interleaved EPI acquisition using an 8-channel receiver coil.

It should be pointed out that the MUSE algorithm is different from existing parallel imaging based motion correction methods that were designed to correct large scale motion in non-diffusion-weighted MRI (Bydder et al. (2003)). In contrast, in this report we mainly address the issues related to shot-to-shot phase inconsistencies in interleaved DWI due to small-scale (e.g., sub-voxel) motions, while assuming that there is no large-scale intrascan motion (i.e., significantly larger than 1 voxel) and the magnitude signals remain constant across multiple EPI segments. This condition is largely met in most of our scans with cooperative subjects. In the presence of very large scale motion, it would be inappropriate to assume that the magnitude signals remain constant across multiple EPI segments. In this case, the MUSE algorithm would need to be further modified or expanded to accommodate for large-scale intrascan motion (Bammer et al. (2007)). It should also be noted that the developed method is designed to address the phase variations among EPI segments, but not those within each individual segment.

Even though the MUSE procedure is only demonstrated with interleaved DWI in this paper, the concept of multiplexed parallel imaging can also be applied to eliminate motion-induced artifacts in interleaved high-resolution DWI and DTI with non-Cartesian k-space trajectories (such as spiral imaging). We expect that MUSE may also be applied to improve the quality for other types of studies where high spatial resolution is desired, such as those in interleaved EPI based functional MRI (fMRI) in the presence of phase variations over time due to physiological motions or magnetic field drifting.

In conclusion, we report in this paper a novel and robust technique to enable high-resolution DWI through a multi-shot acquisition scheme, all inherently without the need for navigator and reference echoes. It is also worth noting that this developed MUSE technique can be readily incorporated with previous advances such as massive parallel imaging to further improve the spatial resolution for DWI. It should thus find broad applications in modern

neuroscience investigations of detailed brain microstructures and related functions where very high spatial resolution is required.

Acknowledgments

This research is supported by NIH Grants R01 NS 074045, R01 EB 009483, R01 NS 075017.

References

Anderson AW, Gore JC. Analysis and correction of motion artifacts in diffusion weighted imaging. Magn Reson Med. Sep; 1994 32 (3):379–87. [PubMed: 7984070]

Andersson JLR, Skare S. A model-based method for retrospective correction of geometric distortions in diffusion-weighted epi. Neuroimage. May; 2002 16 (1):177–99. [PubMed: 11969328]

Atkinson D, Counsell S, Hajnal JV, Batchelor PG, Hill DLG, Larkman DJ. Nonlinear phase correction of navigated multi-coil diffusion images. Magn Reson Med. Nov; 2006 56 (5):1135–9. [PubMed: 16986111]

Atkinson D, Porter DA, Hill DL, Calamante F, Connelly A. Sampling and reconstruction effects due to motion in diffusion-weighted interleaved echo planar imaging. Magn Reson Med. Jul; 2000 44 (1): 101–9. [PubMed: 10893527]

Bammer R, Aksoy M, Liu C. Augmented generalized sense reconstruction to correct for rigid body motion. Magn Reson Med. Jan; 2007 57 (1):90–102. [PubMed: 17191225]

Bammer R, Stollberger R, Augustin M, Simbrunner J, Offenbacher H, Kooijman H, Ropele S, Kapeller P, Wach P, Ebner F, Fazekas F. Diffusion-weighted imaging with navigated interleaved echo-planar imaging and a conventional gradient system. Radiology. Jun; 1999 211 (3):799–806. [PubMed: 10352609]

Basser PJ, Mattiello J, LeBihan D. MR diffusion tensor spectroscopy and imaging. Biophys J. 1994; 66 (1):259–67. [PubMed: 8130344]

Butts K, de Crespigny A, Pauly JM, Moseley M. Diffusion-weighted interleaved echo-planar imaging with a pair of orthogonal navigator echoes. Magn Reson Med. May; 1996 35 (5):763–70. [PubMed: 8722828]

Bydder M, Atkinson D, Larkman DJ, Hill DLG, Hajnal JV. Smash navigators. Magn Reson Med. Mar; 2003 49 (3):493–500. [PubMed: 12594752]

Chen NK, Avram AV, Song AW. Two-dimensional phase cycled reconstruction for inherent correction of echo-planar imaging nyquist artifacts. Magn Reson Med. Oct; 2011 66 (4):1057–66. [PubMed: 21446032]

Farzaneh F, Riederer SJ, Pelc NJ. Analysis of t2 limitations and off-resonance effects on spatial resolution and artifacts in echo-planar imaging. Magn Reson Med. Apr; 1990 14 (1):123–39. [PubMed: 2352469]

Feinberg DA, Moeller S, Smith SM, Auerbach E, Ramanna S, Gunther M, Glasser MF, Miller KL, Ugurbil K, Yacoub E. Multiplexed echo planar imaging for sub-second whole brain fmri and fast diffusion imaging. PLoS One. 2010; 5 (12):e15710. [PubMed: 21187930]

Frank LR, Jung Y, Inati S, Tyszka JM, Wong EC. High efficiency, low distortion 3d diffusion tensor imaging with variable density spiral fast spin echoes (3d dw vds rare). Neuroimage. Jan; 2010 49 (2):1510–23. [PubMed: 19778618]

Griswold MA, Jakob PM, Heidemann RM, Nittka M, Jellus V, Wang J, Kiefer B, Haase A. Generalized autocalibrating partially parallel acquisitions (grappa). Magn Reson Med. Jun; 2002 47 (6):1202–10. [PubMed: 12111967]

Holdsworth SJ, Aksoy M, Newbould RD, Yeom K, Van AT, Ooi MB, Barnes PD, Bammer R, Skare S. Diffusion tensor imaging (dti) with retrospective motion correction for large-scale pediatric imaging. J Magn Reson Imaging. Oct; 2012 36 (4):961–71. [PubMed: 22689498]

Jeong HK, Gore JC, Anderson AW. High-resolution human diffusion tensor imaging using 2-d navigated multishot sense epi at 7 t. Magn Reson Med. May.2012 (E-pub ahead of print).

Jezzard P, Barnett AS, Pierpaoli C. Characterization of and correction for eddy current artifacts in echo planar diffusion imaging. Magn Reson Med. May; 1998 39 (5):801–12. [PubMed: 9581612]

Le Bihan D, Breton E, Lallemand D, Aubin ML, Vignaud J, Laval-Jeantet M. Separation of diffusion and perfusion in intravoxel incoherent motion MR imaging. Radiology. 1988; 168 (2):497–505. [PubMed: 3393671]

Li Z, Pipe JG, Lee CY, Debbins JP, Karis JP, Huo D. X-prop: a fast and robust diffusion-weighted propeller technique. Magn Reson Med. Aug; 2011 66 (2):341–7. [PubMed: 21661046]

Liu C, Bammer R, Kim DH, Moseley ME. Self-navigated interleaved spiral (snails): application to high-resolution diffusion tensor imaging. Magn Reson Med. Dec; 2004 52 (6):1388–96. [PubMed: 15562493]

Miller KL, Pauly JM. Nonlinear phase correction for navigated diffusion imaging. Magn Reson Med. Aug; 2003 50 (2):343–53. [PubMed: 12876711]

Mohammadi S, Möller HE, Kugel H, Müller DK, Deppe M. Correcting eddy current and motion effects by affine whole-brain registrations: evaluation of three-dimensional distortions and comparison with slicewise correction. Magn Reson Med. Oct; 2010 64 (4):1047–56. [PubMed: 20574966]

Moseley ME, Cohen Y, Kucharczyk J, Mintorovitch J, Asgari HS, Wendland MF, Tsuruda J, Norman D. Diffusion-weighted mr imaging of anisotropic water diffusion in cat central nervous system. Radiology. Aug; 1990 176 (2):439–45. [PubMed: 2367658]

Pipe JG, Farthing VG, Forbes KP. Multishot diffusion-weighted fse using propeller mri. Magn Reson Med. Jan; 2002 47 (1):42–52. [PubMed: 11754441]

Porter DA, Heidemann RM. High resolution diffusion-weighted imaging using readout-segmented echo-planar imaging, parallel imaging and a two-dimensional navigator-based reacquisition. Magn Reson Med. Aug; 2009 62 (2):468–75. [PubMed: 19449372]

Pruessmann KP, Weiger M, Scheidegger MB, Boesiger P. Sense: sensitivity encoding for fast mri. Magn Reson Med. Nov; 1999 42 (5):952–62. [PubMed: 10542355]

Reese TG, Heid O, Weisskoff RM, Wedeen VJ. Reduction of eddy-current-induced distortion in diffusion mri using a twice-refocused spin echo. Magn Reson Med. Jan; 2003 49 (1):177–82. [PubMed: 12509835]

Robson MD, Anderson AW, Gore JC. Diffusion-weighted multiple shot echo planar imaging of humans without navigation. Magn Reson Med. Jul; 1997 38 (1):82–8. [PubMed: 9211383]

Rudin L, Osher S, Fatemi E. Nonlinear total variation based noise removal algorithms. Physica D. Nov; 1992 60 (1–4):259–268.

Skare S, Newbould RD, Clayton DB, Bammer R. Propeller epi in the other direction. Magn Reson Med. Jun; 2006 55 (6):1298–307. [PubMed: 16676335]

Turner R, Le Bihan D, Chesnick AS. Echo-planar imaging of diffusion and perfusion. Magn Reson Med. Jun; 1991 19 (2):247–53. [PubMed: 1881311]

Wang FN, Huang TY, Lin FH, Chuang TC, Chen NK, Chung HW, Chen CY, Kwong KK. Propeller epi: an mri technique suitable for diffusion tensor imaging at high field strength with reduced geometric distortions. Magn Reson Med. Nov; 2005 54 (5):1232–40. [PubMed: 16206142]

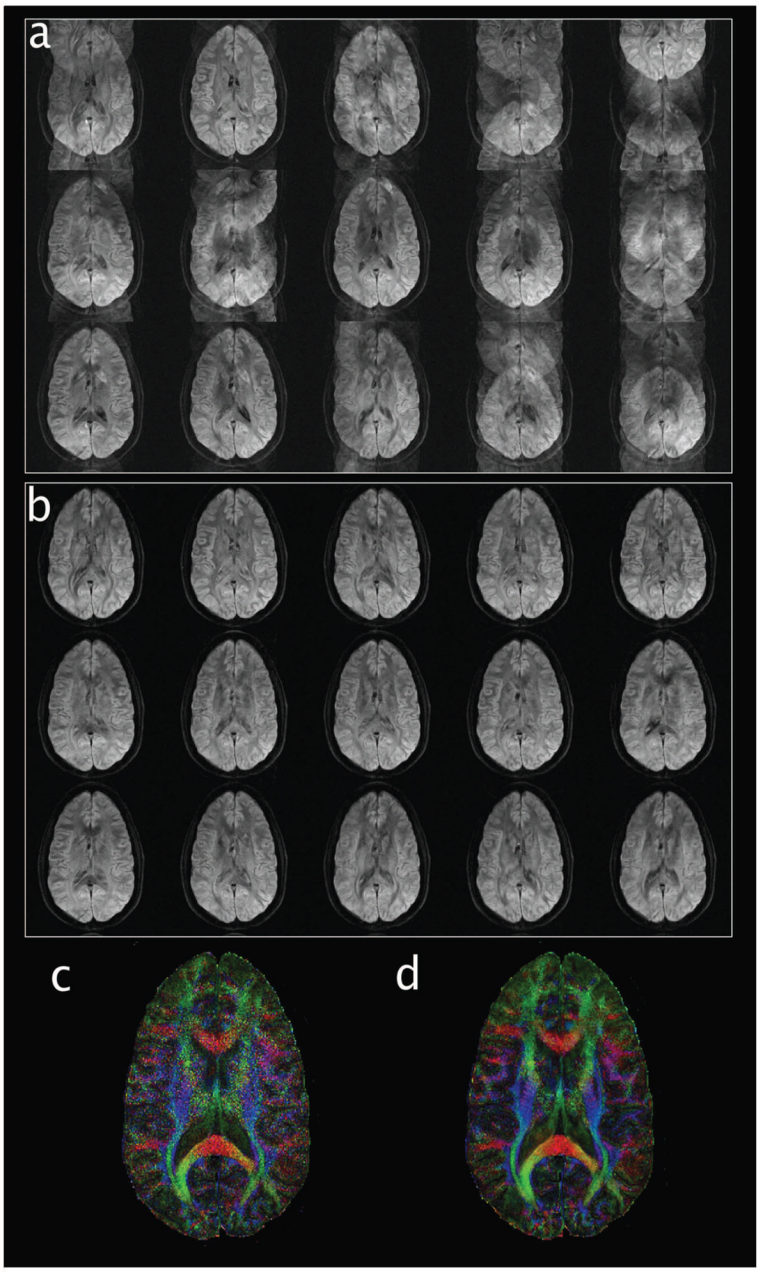

Figure 1.

(a): Four-shot interleaved DTI data ($b=500\frac{sec}{mm^2}$) of 15-direction are susceptible to motion-induced phase errors. (b): Using the MUSE technique, the motion-induced aliasing artifacts can be eliminated. (c): The FA map generated from the conventional SENSE reconstruction has a low SNR. (d): The SNR is improved in FA map produced with the MUSE technique.

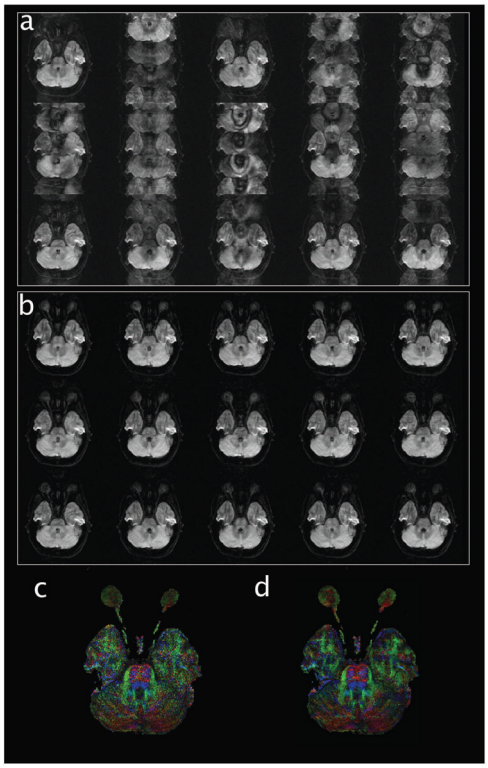

Figure 2.
(a): Pronounced motion-induced artifacts appear in interleaved DTI when there exist local and nonlinear motions (e.g., in the brainstem). (b): The aliasing artifact can be eliminated with the MUSE technique. (c): The SNR is low in the FA map produced with the conventional SENSE procedure. (d): Using the MUSE technique, the FA map of high-SNR can be achieved.

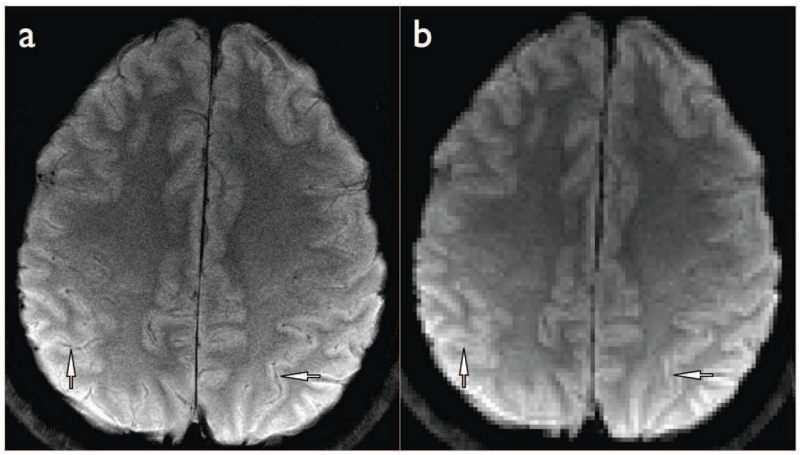

Figure 3.

(a): DWI data of high in-plane resolution (voxel size: $0.375 \times 0.375 \times 5 mm^3$; $b=800 \frac{sec}{mm^2}$) provides good anatomic resolvability. (b): The low-resolution reconstruction of the same data set (voxel size: $1.5 \times 1.5 \times 5 mm^3$) cannot reveal the same anatomic details.

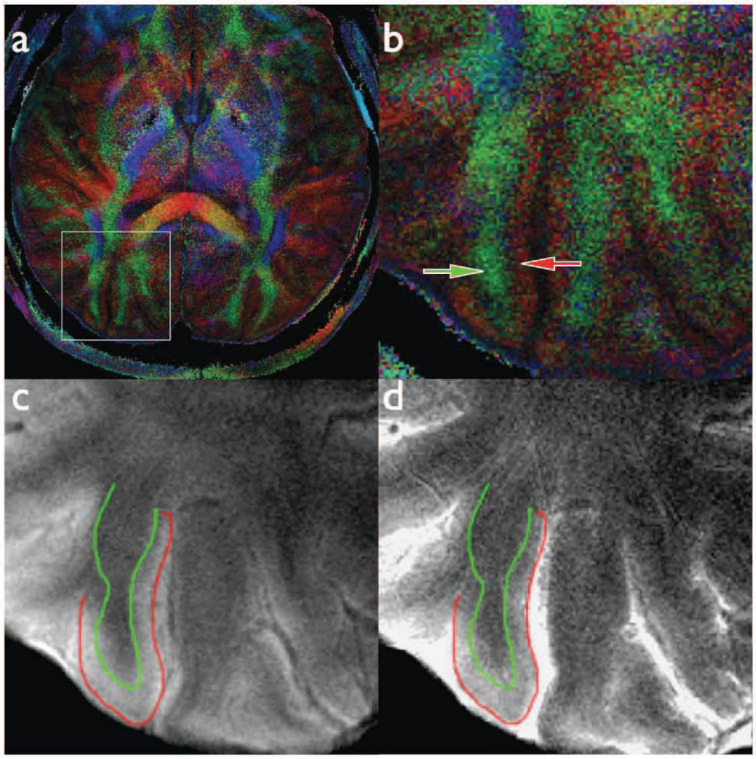

Figure 4.

(a): FA map of high in-plane resolution (voxel size: $0.3 \times 0.3 \times 8 mm^3$; b=$500 \frac{sec}{mm^2}$). (b): FA values for voxels inside the white box of (a). (c) The contour of the indicated green and red voxels in (b) overlaid onto the mean DWI image. (d) The contour of the indicated green and red voxels in (b) overlaid onto the baseline T2-weighted EPI.

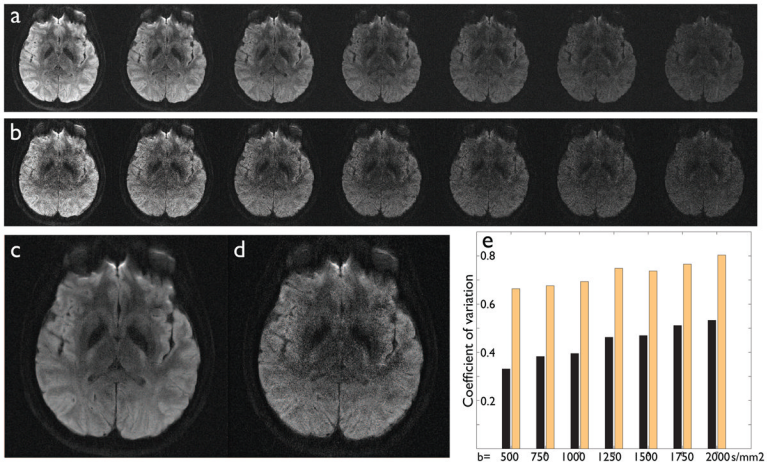

Figure 5.

(a): MUSE-generated DWI corresponding to different b factors (from $500\,\text{to}\,2000\,\frac{sec}{mm^2}$ in a $250\,\frac{sec}{mm^2}$ step). (b): SENSE-generated images of the corresponding b factors (from $500\,\text{to}\,2000\,\frac{sec}{mm^2}$). (c): The magnitude average of all 7 MUSE-generated DWI. (d): The magnitude average of all 7 SENSE-generated DWI. (e) The coefficient of variation measured from white-matter ROIs of MUSE-DWI (black bars) and SENSE-DWI (yellow bars) corresponding to different b factors.